5. Analysis of the effect of tide parameterization on the accuracy of gravity field models

"Whether or not you can observe depends on the theory which you use. It is the theory which decides what can be observed" Albert Einstein.

5.1. Introduction

Gravity field models derived from SLR tracking data are utilized in various fields of research. For instance, they can be used to study the structure of the Earth, for computation of the geoid, reference systems, satellite orbits etc. The quality of the computed satellite orbits depends on the preferred gravity field model and its inherent accuracies. On the other hand, the accuracy of gravity field models is dependent on proper modelling of parameters that describe the disturbing forces acting on a satellite as it orbits the Earth. Factors such as availability, type and quality of data also play a significant role.

The main objective of this chapter is to investigate the contributions of Earth and pole tides on the O-C residuals across selected gravity field models by use of different configurations in the SDAS package. Contributions from the Earth and pole tides on the spherical harmonic coefficients (and also on O-C residuals) are computed using models incorporated into IERS 2010 conventions reported in Petit and Luzum (2010). In the SDAS package the Earth tide model is in the form of three selectable compatible models, these are selectable from the menu as IERS1, IERS2 and IERS3. In SDAS IERS1 corrects Earth tidal effects to degree 2 spherical harmonic coefficients, IERS2 is an extension of IERS1 with further corrections to the third and fourth spherical harmonic coefficients and IERS3 is a complete model which incorporates IERS1, IERS2 and frequency independent components of solid Earth tides.

In this study four SLR parameterization schemes were considered (i.e., the analysis options were configured as IERS1 off, IERS2 off, IERS3 off and pole tides off). The O-C results based on the four different tide parameterization schemes are first characterized by determining the inherent statistical structure. Here a direct comparison of the computed mean SD of the O-C residuals across the different models is used to determine an appropriate model that best describes the O-C data structure. In the second analysis a *t*-test statistical method was used (Student's *t*-test as applied in the *Statistica* statistical analysis package (Motulsky, 2003)) to assess the robustness of the mean SD of the O-C across different tide parameterization tests

based on the selected gravity field models. Overall, the results presented in this chapter have significant implications with regard to the interpretation of the O-C orbit errors computed from different gravity field models using each of the four tide parameterization test models.

5.2. Background

The gravitational attraction of the celestial bodies (e.g., Moon and Sun) exerts a direct force on Earth orbiting satellites. These forces also act on the rotating Earth thereby inducing deformations of the solid Earth. Such deformations tend to produce time variations in surface deflections and gravity with amplitudes up to 50 cm and 200 μGal respectively (Metivier and Conrad, 2008). The motion of the Earth (i.e. in orbit around the Sun and spinning around its instantaneous axis of rotation) and the coupled solar and lunar forces of attraction give rise to tidal deformations. Tidal deformations occur in the solid Earth, the ocean and in the atmosphere. Time varying deformations within the Earth system are consequences of solid Earth tides. On the other hand, pole tides are due to changes in the direction of the Earth's spin axis relative to a certain reference point in the Earth (McCarthy and Petit, 2003, Petit and Luzum 2010).

Generally, Earth and pole tides manifest as time-varying components of the gravity field. As a consequence, the Earth's gravitational field exhibits periodic variations which tend to affect the motion of satellites. Time variations in the global gravity field are often extracted from geodetic satellite data. They are commonly used to study a variety of geodynamic and atmospheric processes. In most geodetic applications, both the solid Earth and pole tides ought to be properly modelled so that their influence can be accounted for in geodetic observables. At present, the solid Earth tide components embedded in spherical harmonic coefficients (geopotential models) are accounted for by using classical models which have been incorporated into various IERS conventions and technical notes, the latest being IERS2010 reported by Petit and Luzum (2010).

5.2.1. Solid Earth tides

5.2.1.1. Effects of solid Earth tides on station coordinates

In SLR analysis the effects of Earth tide deformation are often noticed in the estimated time-varying component of station coordinates (here the greatest influence is in the vertical component of the station coordinates) see for example Figure 16.

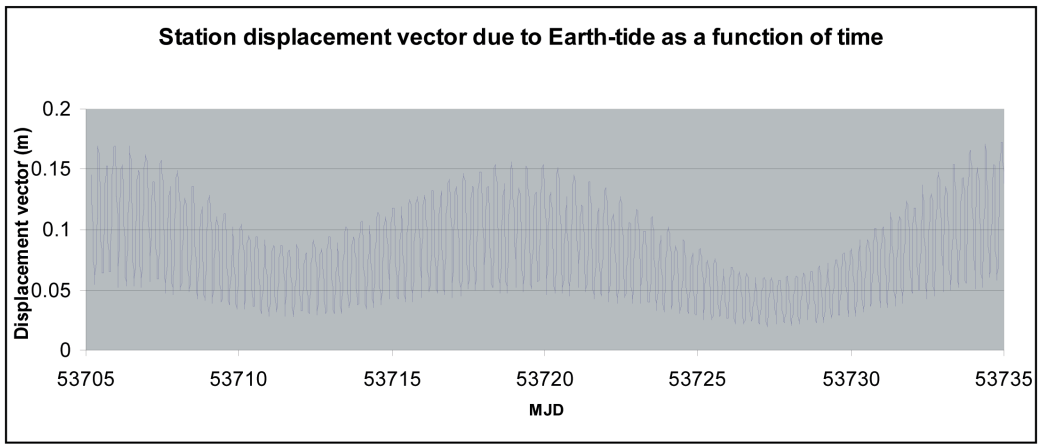

Figure 16. Position displacement of Yarragadee SLR tracking station due to Earth tides (Combrinck and Suberlak, 2007).

The effects of tidal deformations on the station coordinates due to Earth tides are often derived from Equation (71) as reported in Petit and Luzum (2010),

$$\Delta\vec{r} = \sum_{j=2}^{3} \frac{\left[GM_j r^4\right]}{\left[GM_\oplus R_j^{\,3}\right]} \left\{ \left[3l_2\left(\vec{R}_j \cdot \vec{r}\right)\right]\vec{R}_j + \left[3\left(\frac{h_2}{2} - l_2\right)\left(\vec{R}_j \cdot \vec{r}\right)^2 - \frac{h_2}{2}\right]\vec{r} \right\}, \qquad (71)$$

where GM_j and $GM_\oplus$ are the gravitational parameters for the Moon/Sun and the Earth respectively. Similarly, $\vec{R}_j, R_j$ and $\vec{r}, r$ are the unit vectors from the geocentre to the Moon or Sun and to the station respectively, together with the magnitudes of the vectors. In addition, h_2 and l_2 are the nominal second degree Love and Shida numbers respectively.

Tidal deformations are thought to manifest in the station height component since in most geodetic applications nearly all of the parameters in Equation (71) become time-independent at longer time-scales. As a result the time-dependent station height variation due to Earth tide deformations is accounted for by use of Equation (72) (Petit and Luzum, 2010),

$$\delta h_{STA} = \delta h_{K_1} H_{K_1} \left(-\sqrt{\frac{5}{24\pi}} 3 \sin\phi \cos\phi \sin\left(\theta_{K_1} + \lambda\right) \right). \tag{72}$$

In Equation (72) $\delta h_{K_1} = h_{K_1} - h_2$ (the estimated value is -0.0887), H_{K_1} is the amplitude of the K_1 term in the harmonic expansion of the tide generating potential and its value is 0.36878 m, ϕ and λ are the geocentric latitude and east longitude of the station and θ_{K_1} is the K_1 tide argument and is given by $\theta_g + \pi$. Equation (72) can be written in a simplified way as,

$$\delta h_{STA} = -0.0253 \sin\phi \cos\phi \left(\theta_g + \lambda\right). \tag{73}$$

Here the effect is a maximum at $\phi = 45^\circ$ where the amplitude is 0.013 m.

5.2.1.2. Effects of solid Earth tides on geopotential coefficients

The effects of solid Earth tides in the free space potential are often modelled as temporal variations in the standard geopotential coefficients C_{nm} and S_{nm}. Such contributions are often expressed in terms of Love number independence on tidal frequency (this includes long period terms) and station latitude. The effects of ellipticity and rotation of the Earth due to latitudinal dependence and the Coriolis force give rise to tidal deformations. As reported in Wahr (1981), tidal deformation effects require the use of three k- parameters (these are the Love and Shida numbers), k_{nm} and $k_{nm}^{(\pm)}$ (with the exception of $n = 2$) to characterize the changes produced in the free space potential by tides of spherical harmonic of degree and order (nm). In the case where mantle anelasticity is taken into account, anelasticity may introduce small imaginary parts to the k_{nm} and $k_{nm}^{(\pm)}$ terms that reflect a phase lag in the deformation response of the Earth to the tidal forces. In addition, anelasticity may also affect the Earth's deformational response to effects arising from direct action of the tide generating potential (e.g. ocean tides and wobbles of the mantle and the core regions).

The tidal contributions due to Earth tides are accounted for by a two-step formulation reported in Wahr (1981) and Petit and Luzum (2010). In the first step, frequency independent nominal Love numbers are used to evaluate the (nm, for $n = 2$ and $n = 3$ for all m) part of the tidal potential coefficients and compute the corresponding changes $\Delta\bar{C}_{nm}$ and $\Delta\bar{S}_{nm}$ (these are

temporal corrections to geopotential coefficients $\bar{C}_{nm}$ and $\bar{S}_{nm}$) in the time domain using the lunar and solar ephemeris. The induced contributions (i.e. ΔC_{nm} and ΔS_{nm}) due to the nm part of the tidal generating potential in the normalized geopotential coefficients having the same (nm) in the time domain are expressed in terms of the k_{nm} Love number using Equation (74) as reported in Petit and Luzum (2010),

$$\Delta\bar{C}_{nm} - i\Delta\bar{S}_{nm} = \frac{k_{nm}}{2n+1}\sum_{j=2}^{3}\frac{GM_j}{GM_\oplus}\left(\frac{R_e}{r_j}\right)^{n+1} P_{nm}\left(\sin\phi_j\right)e^{-im\lambda_j}. \qquad (74)$$

Here k_{nm} is the nominal Love number for degree n and order m, R_e is the equatorial radius of the Earth, $GM_\oplus$ and GM_j are gravitational parameters for the Earth and the Moon $(j=2)$ or Sun $(j=3)$ respectively, r_j is the distance from geocentre to Moon or Sun and ϕ_j and λ_j are the body-fixed geocentric latitude of the Moon or Sun and east longitude (from Greenwich) of the Sun or the Moon respectively. The contribution to the geopotential coefficients in the degree 4, C_{4m} and S_{nm} due to degree 4 tides are also computed in a similar method in terms of $k_{2m}^{(+)}$ as given in Equation (75),

$$\Delta\bar{C}_{4m} - i\Delta\bar{S}_{4m} = \frac{k_{2m}^{(+)}}{5}\sum_{j=2}^{3}\frac{GM_j}{GM_\oplus}\left(\frac{R_e}{r_j}\right)^{3} P_{2m}\left(\sin\phi_j\right)e^{-im\lambda_j}, \quad (m=0,1,2). \qquad (75)$$

The parameter values utilized in the computation of step 1 are given in Table 16. The nominal value for $m=0$ needs to be selected as a real since the contribution to $\bar{C}_{20}$ from the imaginary part of $k_{20}^{(0)}$.

Table 16. Nominal values of solid Earth tide external potential Love numbers.

Elastic Earth				
n	m	k_{nm}	$k_{nm}^{(+)}$	$R_e k_{nm}$
2	0	0.29525	-0.00087	0.30190
2	1	0.29470	-0.00079	0.29830
2	2	0.29801	0.00057	0.30102
3	0	0.093		
3	1	0.093		
3	2	0.093		
3	3	0.094		

The second step corrects arguments of a harmonic expansion of the tide generating potential for which the error due to the Love number k_2 of step 1 is above a certain cut-off value. In this step the frequency dependent values considered are obtained from Mathews *et al.* (1995) and corrections to $\Delta\bar{C}_{nm}$ and $\Delta\bar{S}_{nm}$ values are from step 1. These corrections are the sum of contributions from a number of tidal constituents belonging to the respective bands. The contribution to $\Delta\bar{C}_{20}$ from the long period tidal constituents of various frequencies, f is given by Equation (76) as reported in Petit and Luzum (2010),

$$R_e \sum_{f(2,0)} \left(A_0 \delta k_f H_f \right) e^{i\theta f} = \sum_{f(2,0)} \left[\left(A_0 H_f \delta k_f^R \right) \cos\theta_f - \left(A_0 H_f \delta k_f^I \right) \sin\theta_f \right]. \quad (76)$$

Furthermore, the contributions to $\left(\Delta\bar{C}_{21} - i\Delta\bar{S}_{21}\right)$ due to the diurnal tidal constituents and to $\left(\Delta\bar{C}_{22} - i\Delta\bar{S}_{22}\right)$ from the semidiurnal band are given by,

$$\Delta\bar{C}_{2m} - i\Delta\bar{S}_{2m} = \eta m \sum_{f(2,m)} \left(A_m \delta k_f H_f \right) e^{i\theta_f}, \qquad (m = 1,2), \qquad (77)$$

where

$$A_0 = \frac{1}{R_e\sqrt{4\pi}} = 4.4228\times10^{-8}\ \mathrm{m}^{-1},$$

$$A_m = \frac{(-1)^m}{R_e\sqrt{8\pi}} = (-1)^m \left(3.1274\times10^{-8}\right)\ \mathrm{m}^{-1}, \qquad (m \neq 0), \qquad (78)$$

$$\eta_1 = -i, \qquad \eta_2 = 1.$$

Here δk_f gives the difference between k_f defined as k_{2m}^0 at frequency f and the nominal value k_{2m}, in the sense $k_f - k_{2m}$ plus a contribution from ocean loading; δk_f^R is the real part of δk_f; δk_f^I is the imaginary part of δk_f; H_f is the amplitude of the term at frequency f from the harmonic expansion of the tide generating potential defined according to the convention of Cartwright and Taylor (1971). In Equation (76),

$$\theta_f = \vec{n}\beta = \sum_{i=1}^{6} n_i \beta_i, \text{ or } \quad \theta_f = m\left(\theta_g + \pi\right) - \vec{N}\vec{F} = m\left(\theta_g + \pi\right) - \sum_{j=1}^{5} N_j F_j.$$

In addition, $\vec{\beta}$ is the six-vector of Doodson's fundamental arguments β_i, (τ, s, h, p, N', p_s), $\vec{n}$ is the six-vector of multipliers n_i of the fundamental arguments, $\vec{F}$ is the five-vector of

fundamental arguments F_j (the Delaunay variables l, l', F, D, Ω) of nutation theory, $\vec{N}$ is the five-vector of multipliers N_j of the Delaunay variables for the nutation of frequency $-f + d\theta_g / dt$ and θ_g is the Greenwich Mean Sidereal Time.

5.2.2. Pole tides

The pole tides cause spatial variations in the gravitational potential due to Earth rotation. These tides are caused by changes in the direction of the Earth's spin axis relative to a point fixed in the Earth. The spin produces a centrifugal force, which depends on the angular distance between the spin axis and a reference point. As the spin axis moves, this distance and the centrifugal force changes. The pole tide deformation effects on the station coordinates (up to ~cm) arises from the first order perturbation associated with the centrifugal potential caused by the Earth's rotation. Rotational deformations due to polar motion can be modelled by assuming that the perturbation in the centrifugal potential is related to the Earth's rotation. Thus considering (x, y, z) as the terrestrial system of reference, a first order perturbation of the centrifugal potential (ΔV) can be expressed in Equation (79), as reported in Petit and Luzum (2010),

$$V = -\frac{1}{2}\left[r^2 \left|\vec{\Omega}\right|^2 - \left(\vec{r}.\vec{\Omega}\right)^2 \right], \tag{79}$$

where $\vec{\Omega} = \Omega\left(m_1 \hat{x} + m_2 \hat{y} + \left(1 + m_3\right)\hat{z}\right)$, Ω is the mean angular velocity of rotation of the Earth, m_1 and m_2 are small dimensionless parameters describing the time dependent offset of the instantaneous rotation pole from the mean, m_3 is the fractional variation in the rotational rate, r is the geocentric distance to the station. Neglecting the m_3 term, due to its small influence, the first order perturbation in the potential (ΔV) can be written in terms of m_1 and m_2 as in Equation (80) (Petit and Luzum, 2010),

$$\Delta V\left(r, \theta, \lambda\right) = -\left(\frac{\Omega^2 r^2}{2}\right)\sin 2\theta\left(m_1 \cos\lambda + m_2 \sin\lambda\right). \tag{80}$$

The tidal Love numbers and ΔV can be used to compute the radial (S_r, positive upwards) and horizontal displacements S_θ and S_λ (positive southwards and eastwards respectively) due to ΔV as given in Equation (81),

$$S_r = h_2 \frac{\Delta V}{g}, \quad S_\theta = \frac{l_2}{g} \partial_\theta \Delta V, \quad S_\lambda = \frac{l_2}{g} \frac{1}{\sin\theta} \partial_\lambda \Delta V. \tag{81}$$

The coordinates (in the ITRF) of the position of the Earth's mean rotation pole due to secular variations are given in terms of the polar motion variables (x_p, y_p) and are obtained by running averages $\bar{x}_p$ and $-\bar{y}_p$, thus

$$m_1 = x_p - \bar{x}_p, \qquad m_2 = -\left(y_p - \bar{y}_p\right). \tag{82}$$

In order to achieve the most accurate results for the polar motion variables estimates of the mean pole are commonly utilised. Now-a-days the conventional mean pole of the IERS conventions (2003) is replaced with the IERS conventional mean pole incorporated in the IERS conventions (2010). The latest version of the IERS conventional mean pole is composed of a cubic model validated over the period from 1976.0 to 2010.0 and a linear model for extrapolation after 2010.0. Generally, the IERS (2010) mean pole model can be described as per Equation (83)

$$\bar{x}_p(t) = \sum_{i=0}^{3} (t - t_0)^i \times \bar{x}_p^i \qquad \bar{y}_p(t) = \sum_{i=0}^{3} (t - t_0)^i \times \bar{y}_p^i, \tag{83}$$

where t_0 is 2000 and the coefficients of $\bar{x}_p^i$ and $\bar{y}_p^i$ are given in Table 17.

Table 17. Coefficients of the IERS (2010) mean pole model.

Degree i	Until 2010.0		After 2010.0	
	$\bar{x}_p^i$ / mas yr^{-i}	$\bar{y}_p^i$ / mas yr^{-i}	$\bar{x}_p^i$ / mas yr^{-i}	$\bar{y}_p^i$ / mas yr^{-i}
0	55.974	346.346	23.513	358.891
1	1.8243	1.7896	7.6141	-0.6287
2	0.18413	-0.10729	0.0	0.0
3	0.007024	-0.000908	0.0	0.0

The radial and horizontal displacements S_r, S_θ and S_λ, can be computed by use of Love number values appropriate to the frequency of the pole tides $(h = 0.6027,\ l = 0.0836)$ and $r = a = 6.378 \times 10^6$ m as follows:

$$\begin{aligned} S_r &= -32 \sin 2\theta \left(m_1 \cos\lambda + m_2 \sin\lambda\right) \text{ mm}, \\ S_\theta &= -9 \cos 2\theta \left(m_1 \cos\lambda + m_2 \sin\lambda\right) \text{ mm}, \\ S_\lambda &= 9 \cos 2\theta \left(m_1 \sin\lambda - m_2 \cos\lambda\right) \text{ mm}, \end{aligned} \tag{84}$$

with m_1 and m_2 given in arcseconds. The effects of polar motion in the Cartesian coordinate systems as reported in IERS2010 conventions (Petit and Luzum, 2010) are represented in Equation (85),

$$\left[dX, dY, dZ\right]^T = R^T \left[S_\theta, S_\lambda, S_r\right]^T, \tag{85}$$

where

$$R = \begin{pmatrix} \cos\theta\cos\lambda & \cos\theta\sin\lambda & -\sin\theta \\ -\sin\lambda & \cos\lambda & 0 \\ \sin\theta\cos\lambda & \sin\theta\sin\lambda & \cos\theta \end{pmatrix}. \tag{86}$$

In order to show the effects of pole tides to the accuracy of gravity field models Equation (80) can be expressed as Equation (87)

$$\Delta V\left(r,\theta,\lambda\right) = -\frac{\Omega^2 r^2}{2}\sin 2\theta R_e\left[\left(m_1 - im_2\right)e^{i\lambda}\right]. \tag{87}$$

The deformation caused by the pole tide produces time-dependent perturbations in the external potential given by Equation (88)

$$\Delta V = -\frac{\Omega^2 r^2}{2}\sin 2\theta R_e\left[k_2\left(m_1 - im_2\right)e^{i\lambda}\right]. \tag{88}$$

These perturbations are related to changes in the geopotential coefficients C_{21} and S_{21}, which describe the position of the Earth's figure axis. Using the value $0.3077 + 0.0036i$ for the Love number k_2 the time-dependent perturbations in the C_{21} and S_{21} geopotential coefficients can be estimated as follows

$$\begin{aligned} \Delta\bar{C}_{21} &= -1.333\times10^{-9}\left(m_1 - 0.0115m_2\right), \\ \Delta\bar{S}_{21} &= -1.333\times10^{-9}\left(m_1 - 0.0115m_2\right), \end{aligned} \tag{89}$$

where m_1 and m_2 given in arcseconds.

5.3. Parameterization

The latest SDAS version (Combrinck personal communication, July 2012) utilises IERS2010 conventions to correct for Earth and pole tide effects. In the software the Earth tide model is divided into three compatible and selectable models namely, IERS1, IERS2 and IERS3 (these are described in Table 18). The objective of the work presented in this chapter is to perform orbital tests with particular emphasis on evaluating the influence of using IERS1, IERS2 and

IERS3 compatible Earth tide models (affecting the static GGM spherical harmonic coefficients) and pole tide model (IERS2010 standard) in the determination of satellite orbits by analysing LAGEOS data using different gravity field models. The IERS1 model in SDAS is considered the least complex Earth tide model and corrects degree 2 spherical harmonics of a given geopotential model. On the other hand, IERS2 in the analysis software is an extension of IERS1 with additional corrections to third and fourth degree spherical harmonics. Lastly, a complete model of Earth tides, the IERS3 is considered as the most complex model since it includes both IERS1 and IERS2 plus it takes into account the frequency independent components of the solid Earth tides. A summary of these compatible models and their respective corrections to spherical harmonic coefficients is given in Table 18.

Table 18. Summary of the compatible models derived from IERS2010 with their respective corrections to spherical harmonic coefficients of a geopotential model.

Compatible models from IERS2010	Corrections to a typical geopotential model
IERS1	$C_{20}, C_{21}, C_{22}, S_{21}, S_{22}$
IERS2	IERS1 + $C_{30}, C_{31}, C_{32}, C_{33}, S_{31}, S_{32}, S_{33}$ + $C_{40}, C_{41}, C_{42}, S_{41}, S_{42}$
IERS3	IERS1 + IERS2 + frequency independent components
Pole tides	C_{21}, S_{21}

The methodology followed can be formulated as follows: suppose that a GGM is represented by $y = \eta(x)$, where x represents a vector of input empirical models to be varied and y is the expected output; for the purpose of this study y is considered as the O-C residuals. Let η be a GGM such that the way the model responds to changes in each of the three elected empirical models is not transparent. The purpose of selecting different empirical model combinations during the analysis of SLR data is to investigate how changes in the geopotential coefficients (GGM dependent) in the context of O-C residuals, y, are related to or affected by Earth (as modelled by IERS1, IERS2 and IERS3) and pole tides (modelled using IERS2010 standard) contributions.

Table 19 summarises the criteria used to test the effects of the IERS1, IERS2, IERS3 and pole tides on the O-C residuals across five different gravity field models when determining LAGEOS orbits as analysed with SDAS. In particular, the "on/disabled" configuration tests were conducted for each considered model by disabling one of the compatible models while the

other two are enabled during processing. Basically four tests were conducted for each selected gravity field model based on LAGEOS 1 and 2 data. In the first test the IERS1 Earth tide model and pole tides (IERS2010 standard) were activated while disabling IERS2 and IERS3 in the software. The second test involved the activation of IERS2 and pole tides while IERS3 was disabled in the software to investigate their combined effects on the derived O-C residuals across the selected models. In third test the IERS3 and pole tides were implemented and lastly, in the fourth test the IERS3 was activated and pole tides were disabled during LAGEOS 1 and 2 data processing.

Table 19. Orbital parameter tests strategy used. Parameters were tested at 0.8σ rejection.

Orbital tests	Parameter configuration	
Test 1	IERS1 and pole tides 'on'	IERS2 and IERS3 'disabled'
Test 2	IERS2 and pole tides 'on'	IERS3 'disabled'
Test 3	IERS3 and pole tides 'on'	IERS1 and IERS2 'enabled'
Test 4	IERS3 'on'	Pole tides 'disabled'

5.4. Models Evaluated

In this study five gravity field models were used in SDAS analysis of LAGEOS 1 and 2 SLR data. These models are the GRIM5C1, EIGEN-CG30C, AIUB-CHAMP01S, EGM2008 and AIUB-GRACE01S and they were evaluated using LAGEOS 1 and 2 data sets spanning January to June 2009. Specific characteristics and references of the selected models are summarized in Table 20. The ILRS tracking stations selected for data processing are the so-called EOP SLR stations. These stations are believed to be providing high quality SLR data for the computation of EOPs. The EOP selected stations include Yarragadee, McDonald, Zimmerwald, Wettzell, Monument Peak, Hartebeesthoek, Herstmonceux, Greenbelt, Riyadh, Graz, Mount-Stromlo, Beijing and Arequipa.

Table 20. Geopotential models evaluated.

Model	Year	Degree/order	Data	Reference
GRIM5C1	1999	120	S, G, A	Gruber *et al.* (2000)
EIGEN-CG03C	2005	360	S(CHAMP,GRACE),G,A	Foerste *et al.* (2005)
AIUB-CHAMP01S	2007	90	S(CHAMP)	Prange *et al.* (2007)
EGM2008	2008	2190	S(GRACE),G,A	Pavlis *et al.* (2008)
AIUB-GRACE01S	2008	120	S(GRACE)	Jaeggi *et al.* (2008)

The SLR data in this study were processed using constants and reference frames listed in Table 21.

Table 21. Constants and reference frames utilised during LAGEOS 1 and 2 data processing.

Reference frame epoch	SLRF2005
Inertial reference frame	J2000
Pole-tide correction (station position)	IERS2010
Correction for general relativistic effects	IERS2010
Earth–tide correction (station position)	Petrov 2005
Ocean loading correction (station position)	Agnew/Scherneck
Atmospheric loading	Disabled
Earth orientation	a-priori Earth orientation parameters and UTC-UT1 values as per IERS extrapolated to observation epoch
O-C outlier rejection	Selectable: set to 0.8 sigma
Average pole	IERS2010

5.5. Statistical analysis of O-C residuals

Table 22 and Table 23 present the results for the statistical orbital fits of LAGEOS 1 and 2 based on IERS1, IERS2, IERS3 and pole tide tests using the GRIM5C1, EIGEN-CG03C, AIUB-CHAMP01S, EGM2008 and AIUB-GRACE01S gravity field models. The listed statistical results considered in the tables are the mean SD of the O-C residuals for each orbital test. These SD values are used as a measure of orbit quality as well as gravity model accuracy. There are small differences in the calculated average SDs across the five elected gravity field models. This suggests that the choice of parameterizations has a particular influence on satellite orbit determination as well as gravity field model accuracy. The results presented in Table 22 and Table 23 indicate that from the SLR analysis utilizing the selected gravity field models, the average SDs of the O-C residuals are about 2 cm and 1 cm for LAGEOS 1 and 2 respectively.

The following five GGM model comparisons utilised LAGEOS 1 data.

GRIM5C1:

In Table 22 the GRIM5C1 gravity field model gives a slightly improved solution when the Earth tides are modelled using the complex Earth tide model, IERS3, with the pole tides disabled

during data processing followed by a combined implementation of the IERS3 model and pole tides. A combination of the IERS2 model and pole tides decreases the quality of the GRIM5C1 gravity field model. The poorest O-C SD solution is obtained when the least complex Earth tide model IERS1 and pole tides are jointly implemented in the software. This indicates that the accuracy of the final solution when using the GRIM5C1 model and LAGEOS 1 data can be achieved through inclusion of spherical harmonic components due to Earth tides (added) to those of the GRIM5C1 model. The pole tides seem to contribute less towards the precision of the final solution of GRIM5C1.

EIGEN-CG03C:

The combined gravity field model, EIGEN-CG03C gives the best solution for the combined selection of IERS3 and pole tides followed by a combination of IERS2 and pole tides. The O-C SD solution worsens when IERS3 is activated and pole tides disabled in SDAS. Its worst solution is when IERS1 and pole tides are jointly selected during data processing. Based on this result the Earth and pole tides equally contribute towards the quality of the EIGEN-CG03C gravity field model. Hence it is necessary to include both the spherical harmonic coefficient components due to the Earth and pole tides when using EIGEN-CG03C and LAGEOS 1 data.

AIUB-CHAMP01S:

The CHAMP satellite-only model, AIUB-CHAMP01S results in a better solution when IERS3 and pole tides are jointly active in the software followed by when the IERS3 model is active and pole tides disabled. The solution worsens when IERS2 and pole tides are jointly selected and the poorest solution is obtained when the least complex Earth tide model, IERS1 and pole tides are jointly selected. In conjunction with the EIGEN-CG03C gravity field, the usage of AIUB-CHAMP01S with LAGEOS 1 data requires the inclusion of both the spherical harmonic coefficient components due to Earth and pole tides.

EGM2008:

For the EGM2008 gravity field model the best solution is obtained when IERS2 and pole tides are active, followed by the combination of IERS3 and pole tides. The average SD of the O-C residuals reduces when the IERS1 model and pole tides are active during data processing. Its

poorest solution is obtained when the IERS3 model is active and the pole tides disabled in SDAS. The results indicate that both the spherical harmonic coefficient components due to Earth and pole tides play a significant (interacting) role in the final solution of the EGM2008 gravity field model when LAGEOS 1 data is utilised.

AIUB-GRACE01S:

Lastly using LAGEOS 1, the GRACE satellite-only model AIUB-GRACE01S, exhibits the best solution when the IERS3 model is activated and pole tides are disabled in the software followed by a combined implementation of IERS3 and pole tides. The O-C SD solution worsens when IERS2 and pole tides are implemented during data processing. The worst solution is obtained when the least complex Earth tide model, IERS1 and pole tides are implemented in SDAS. This suggests that optimal use of the quality of AIUB-GRACE01S occurs when using LAGEOS 1 data through a proper and a complete modelling of contributions from Earth tides only. The differences between IERS1, IERS2 and IERS3 O-C values are statistical only, as the differences are non-significant (at the level of fractions of mm).

Table 22. Results of the mean SD of the O-C extracted from LAGEOS 1 data.

Model	Mean SD [cm] when IERS1 and pole tides are 'on'	Mean SD [cm] when IERS2 and pole tides are 'on'	Mean SD [cm] when IERS3 and pole tides are 'on'	Mean SD [cm] when IERS3 is 'on' & pole tides are disabled
GRIM5C1	2.184	2.151	2.131	2.129
EIGEN-CG03C	2.308	2.266	2.246	2.279
AIUB-CHAMP01S	2.187	2.135	2.116	2.126
EGM2008	2.202	2.160	2.169	2.165
AIUB-GRACE01S	2.174	2.145	2.141	2.133

Figure 17 depicts SD values averaged across the selected (five) gravity field models for individual tide parameterization test. As depicted in Figure 17 the IERS1 and pole tides test exhibits the highest mean SD solution while the mean SD of the O-C improves for the three remaining parameterization tests with only parts-per millimetre differences. In particular, the IERS3 and pole tide parameterization test have the lowest solution. This is expected since most

of the gravity field models yield a best mean SD solution when IERS3 and pole tides are activated during the LAGEOS 1 data processing.

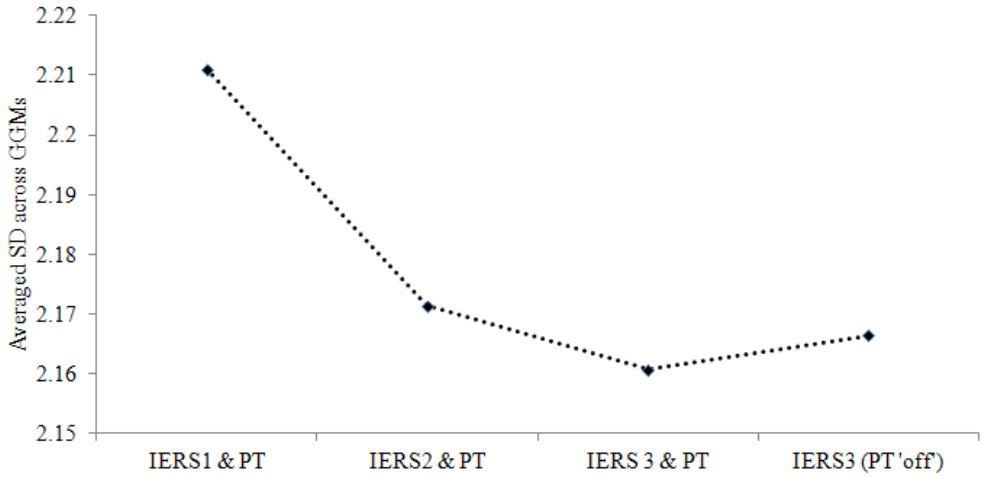

Figure 17. Averaged SD across the GRIM5C1, EIGEN-CG03C, AIUB-CHAMP01S, EGM2008 and AIUB-GRACE01S gravity field models based on LAGEOS 1 data.

The following five GGM model comparisons utilised LAGEOS 2 data.

GRIM5C1:

The GRIM5C1 gravity field model has the lowest O-C SD solution when LAGEOS 2 data are processed with IERS3 and pole tides activated followed by active combination of IERS2 and pole tides in SDAS. The solution worsens when the IERS3 model is active and the pole tides are disabled during data processing. The poorest O-C SD solution is obtained when the least complex Earth tide model, IERS1 and pole tides are jointly activated in the software. Similar to the results obtained for LAGEOS 1, the optimal use of the quality of GRIM5C1 when using LAGEOS 2 occurs when all spherical harmonic functions due to the Earth and pole tides are included to those of the gravity field model. The different O-C SD values obtained for LAGEOS 1 where pole tide was either on or off, combined with IERS3 are statistically insignificant. Therefore one would want to utilise IERS3 and pole tides for both LAGEOS 1 and LAGEOS 2 when using GRIM5C1.

EIGEN-CG03C:

The combined gravity field model, EIGEN-CG03C exhibits the best O-C SD solution when the IERS3 model is active with pole tides disabled followed by the active combination of IERS2 and pole tides in the software. The solution worsens with the joint combination of IERS1 and pole tides and the poorest solution is obtained when IERS3 and pole tides are jointly selected during LAGEOS 2 data processing. This result is different from the previous EIGEN-CG03C using LAGEOS 1 data. It is apparent that adding the spherical harmonic coefficients to those of the GGM due to pole tide in combination with the IERS3 Earth tide coefficients reduces the quality of the solution.

AIUB-CHAMP01S:

The CHAMP satellite-only model has the best solution when IERS3 and pole tides are active in SDAS followed by the implementation of IERS3 with pole tides disabled. A combination of IERS2 and pole tides reduces the quality of the O-C SD solution. The solution worsens further when the least complex Earth tide model, IERS1 and pole tides are jointly combined in the software. This is similar result obtained with AIUB-CHAMP01S using LAGEOS 1 data implying that there are no satellite dependence effects. Considering the similarities in the results from the two satellites it can be concluded that the full spherical harmonic coefficient components due to the Earth and pole tides need to be taken into account when using AIUB-CHAMP01S and LAGEOS 2.

EGM2008:

The EGM2008 gravity field model exhibits the lowest O-C SD solution when IERS3 and pole tides are selected, followed by the active combination of IERS2 and pole tides during LAGEOS 2 data analysis. Activation of the complex Earth tide model, IERS3 with the pole tides disabled worsens the O-C SD solution. The poorest solution is obtained when the IERS1 model and pole tides are jointly selected in the software. Considering the results obtained with LAGEOS 1 data, this indicates the necessity of including the full spherical harmonic coefficient components due to pole tides when using EGM2008 and LAGEOS 1 and 2 data. In both cases (LAGEOS 1 and LAGEOS 2) results are improved when including pole tides.

AIUB-GRACE01S:

The GRACE satellite-only model, AIUB-GRACE01S gives the best solution when contributions from the Earth tides are modelled with IERS 3 while the pole tides are disabled, followed by the active combination of IERS2 and pole tides in the software. A joint implementation of the complex Earth tide mode with pole tides reduces the O-C SD solution. The solution worsens further with active combination of the least complex Earth tide model, IERS1 and pole tides. Considering the quality of AIUB-GRACE01S it is necessary to include spherical harmonic coefficient components due Earth tides when using LAGEOS 2 data. It is also apparent that the inclusion of spherical harmonic coefficient components due pole tides tends to reduce the quality of the AIUB-GRACE01S gravity field model although this is at such a low level to be statistically insignificant.

Table 23. Results of the mean SD extracted from LAGEOS 2 data for different tide parameterization options.

Model	Mean SD [cm] when IERS1 and pole tides are 'on'	Mean SD [cm] when IERS2 and pole tides are 'on'	Mean SD [cm] when IERS3 and pole tides are 'on'	Mean SD [cm] when IERS3 is 'on' and pole tides are disabled
GRIM5C1	1.490	1.467	1.463	1.486
EIGEN-CG03C	1.711	1.634	1.828	1.633
AIUB-CHAMP01S	1.515	1.500	1.490	1.498
EGM2008	1.524	1.497	1.483	1.510
AIUB-GRACE01S	1.527	1.481	1.495	1.469

The trend of the averaged SD of the O-C residuals for the four parameterization tests across all the considered gravity field models based on LAGEOS 2 data is illustrated in Figure 18. Highest averaged mean SD solutions are obtained for IERS1 and pole tides, and IERS3 and pole tides parameterization tests. The results obtained for the IERS3 and pole tides test contradicts those obtained when LAGEOS 1 SLR data is utilized (here IERS3 and pole tides gave the best mean SD solution). This difference arises from the large mean SD of the O-C residuals obtained when using the EIGEN-CG03C gravity field model while processing SLR LAGEOS 2 data. Generally the IERS3 and pole tides parameterization with the EIGEN-CG03C gravity field model based on the analysis of LAGEOS 2 SLR data yields O-C residuals which are almost twice as large as

compared with those obtained from the other parameterization test for the similar model and data. This uniqueness could be attributed to systematic errors in the adjustment procedure during data processing. It is apparent that the pole tides have a significant influence on the final O-C residual, considering the IERS3 Earth tide model and the EIGEN-CG03C gravity field model. If the average O-C value of the EIGEN-CG03C model is excluded, the plot in Figure 18 would be similar to that of Figure 17, with the least detailed model exhibiting the largest O-C values and the most detailed model (IERS3 plus pole tide) providing the best solutions as depicted in Figure 19. This example indicates that some GGM models may produce unexpected results.

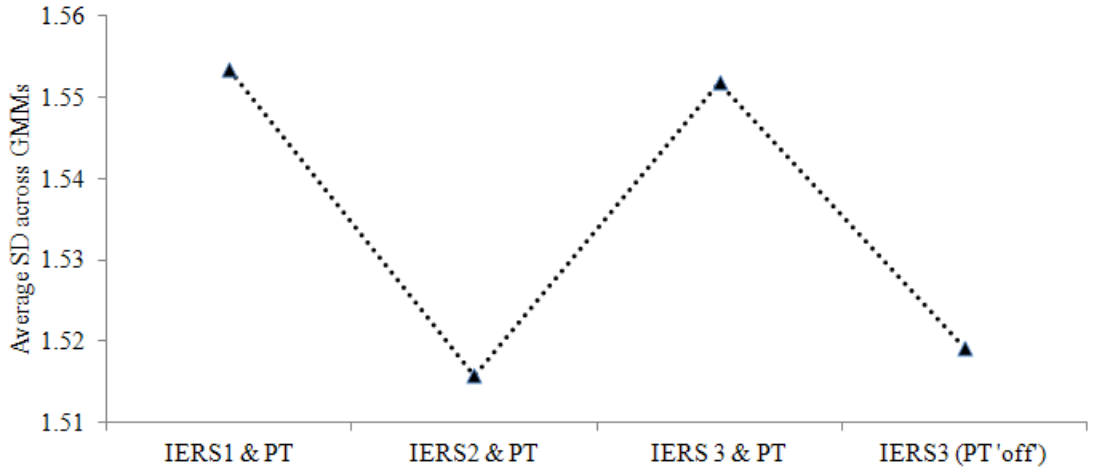

Figure 18. Averaged SD across GRIM5C1, EIGEN-CG03C, AIUB-CHAMP01S, EGM2008 and AIUB-GRACE01S gravity field models based on LAGEOS 2 data.

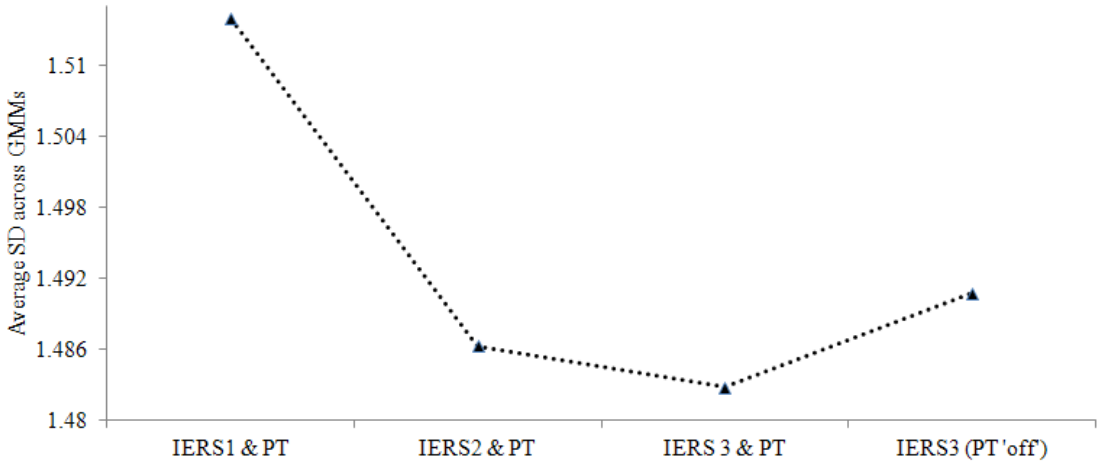

Figure 19. Averaged SD across GGMs with EIGEN-CG03C model excluded.

5.6. Statistical significance of the variations in the standard deviation of O-C residuals between models

The mean SD of the O-C residuals presented in Table 22 and Table 23 as derived from LAGEOS 1 and 2 data using GRIM5C1, EIGEN-CG03C, AIUB-CHAMP01S, EGM2008 and AIUB-GRACE01S gravity field models exhibit subtle differences across the different tide parameterization. This makes it difficult to ascertain whether the difference in the mean SD values has any statistical significance for the different gravity field models. In this section a *t*-test was performed to assess whether the mean SD differences between the tide parameterization options are statistically different from each other. In particular the mean SD of two groups of tide parameterization tests is compared to investigate whether the means are statistically significant.

The *t*-test (Welch's t-test) used in the present study was computed as a ratio of the difference between the two averages and the measure of O-C residual variances corresponding to the different parameterization options. If the parameter options are i and j then the student's t-test can be calculated as per Equation

$$t_{ij/ji} = \frac{\bar{X}_i - \bar{X}_j}{\sqrt{\frac{S_i^2}{N_i} - \frac{S_j^2}{N_j}}}, \qquad \forall\ i \neq j \tag{90}$$

where $\bar{X}_i$ and $\bar{X}_j$ are the means of the i and j O-C residuals, S_i^2 and S_j^2 are the pooled O-C residual variances, N_i and N_j are the data sizes for test i and test j and $t_{ij/ji}$ is the test statistic evaluated as a Student t quantile with $N_i + N_j - 2$ degrees of freedom. In this study a risk or significant level given by $\alpha = 0.05$ is used to test for significance between two considered groups. For example if a typical *t*-test gives a *p*-value less than or equal to 0.05 $(p \leq 0.05)$ then the mean SD difference between the two is deemed statistically significant else it is statistically insignificant. The results for the *t*-tests performed using the O-C residuals derived from the four tide parameterization tests using the GRIM5C1 gravity field model during the analysis of SLR data derived from LAGEOS 1 observations are summarised in Table 24 (differences are in metres). Here the variables considered correspond to the orbital tests summarised in Table 19, that is, Var 1: IERS1 and pole tides; Var 2: IERS2 and pole tides; Var 3: IERS3 and pole tides

and Var 4 corresponds to the IERS3 test with the pole tides disabled. In Table 24 the *t*-test computed between Var 1 and Var 2, Var 1 and Var 3, Var 1 and Var 4, Var 3 and Var 4 have *p*-values that are greater than the 0.05 (or 5%) significance level implying that the differences in the mean SD (listed in column 2) are not statistically significant. In contrast the computed *t*-values for Var 2 versus Var 3 and Var 2 versus Var 4 correspond to *p*-values which are less than 0.05 implying that the difference in the mean SD between the considered group tests for GRIM5C1 are statistically significant.

Table 24. The *t*-test results for GRIM5C1 based on LAGEOS 1 data.

Variable	Diff (mean SD)	Diff. (SD)	t-value	p-value
Var 1 vs. Var 2	0.000330	0.005756	0.75404	0.451857
Var 1 vs. Var 3	0.000537	0.005795	1.21940	0.224362
Var 1 vs. Var 4	0.000550	0.005774	1.25360	0.211690
Var 2 vs. Var 3	0.000207	0.001279	2.13114	0.034498
Var 2 vs. Var 4	0.000220	0.001466	1.97644	0.049704
Var 3 vs. Var 4	0.000013	0.001652	0.10385	0.917410

Table 25 (difference values are in metres) summarises the *t*-test results for EIGEN-CG03C using LAGEOS 1 data. Considering the *p*-values calculated in each of the tests it is apparent that the mean SD differences between the considered group tests are statistically insignificant. The negative *t*-test value implies that the first mean was smaller than the second mean for the considered groups. Similar results are obtained for the three remaining gravity field models (AIUB-CHAMP01S, EGM2008 and AIUB-GRACE01S) though the p-values are relatively low, see Table 26, Table 27 and Table 28.

Table 25. The *t*-test results for EIGEN-CG03C based on LAGEOS 1 data.

Variable	Diff (mean SD)	Diff. (SD)	*t*-value	*p*-value
Var 1 vs. Var 2	0.000421	0.010541	0.51030	0.610537
Var 1 vs. Var 3	0.000617	0.010592	0.74423	0.457818
Var 1 vs. Var 4	0.000294	0.010954	0.34250	0.732420
Var 2 vs. Var 3	0.000196	0.002346	1.06703	0.287547
Var 2 vs. Var 4	-0.000127	0.002695	-0.60382	0.546807
Var 3 vs. Var 4	-0.000324	0.002621	-1.57596	0.116985

Table 26. The *t*-test results for AIUB-CHAMP01S based on LAGEOS 1 data.

Variable	Diff (mean SD)	Diff. (SD)	*t*-value	*p*-value
Var 1 vs. Var 2	0.000514	0.005443	1.24209	0.215896
Var 1 vs. Var 3	0.000705	0.005664	1.63682	0.103497
Var 1 vs. Var 4	0.000611	0.005695	1.41097	0.160061
Var 2 vs. Var 3	0.000191	0.001520	1.65192	0.100375
Var 2 vs. Var 4	0.000097	0.001472	0.86594	0.387728
Var 3 vs. Var 4	-0.000094	0.001930	-0.64046	0.522728

Table 27. The *t*-test results for EGM2008 based on LAGEOS 1 data.

Variable	Diff (mean SD)	Diff. (SD)	*t*-value	*p*-value
Var 1 vs. Var 2	0.000420	0.006054	0.911976	0.363058
Var 1 vs. Var 3	0.000322	0.006073	0.697232	0.486599
Var 1 vs. Var 4	0.000368	0.006332	0.763458	0.446236
Var 2 vs. Var 3	-0.000098	0.001810	-0.710726	0.478217
Var 2 vs. Var 4	-0.000052	0.001433	-0.479173	0.632424
Var 3 vs. Var 4	0.000046	0.001909	0.314152	0.753786

Table 28. The *t*-test results for AIUB-GRACE01S based on LAGEOS 1.

Variable	Diff (mean SD)	Diff. (SD)	*t*-value	*p*-value
Var 1 vs. Var 2	0.000289	0.002903	1.30929	0.192183
Var 1 vs. Var 3	0.000326	0.002355	1.81808	0.070791
Var 1 vs. Var 4	0.000409	0.003055	1.75956	0.080260
Var 2 vs. Var 3	0.000036	0.002757	0.17405	0.862027
Var 2 vs. Var 4	0.000120	0.001508	1.04348	0.298192
Var 3 vs. Var 4	0.000083	0.002864	0.38196	0.702960

The *t*-test results for the GRIM5C1 gravity field model using LAGEOS 2 data are given in Table 29. The computed *t*-values for all the six pairs give *p*-values are greater than the 0.05 risk level. It is therefore concluded that the computed mean SD differences between these six group tests are not statistically significant.

Table 29. The *t*-test results for GRIM5C1 based on LAGEOS 2 data.

Variable	Diff (mean SD)	Diff. (SD)	*t*-value	*p*-value
Var 1 vs. Var 2	0.000230	0.008858	0.32710	0.744027
Var 1 vs. Var 3	0.000269	0.009625	0.35287	0.724659
Var 1 vs. Var 4	0.000039	0.009065	0.05406	0.956954
Var 2 vs. Var 3	0.000040	0.002298	0.21727	0.828282
Var 2 vs. Var 4	-0.000191	0.001383	-1.74026	0.083761
Var 3 vs. Var 4	-0.000230	0.002202	-1.32019	0.188680

Table 30 summarises the *t*-test results for the EIGEN-CG03C model based on LAGEOS 2 data. Based on the results presented in Table 30 there are no statistically significant differences in the mean SD between Var 1 versus Var 2, Var 1 versus Var 3, Var 1 versus Var 4 and Var 2 versus Var 4 tests (since $p \geq 0.05$). In contrast the computed *t*-values between Var 2 versus Var 3 and Var 3 versus Var 4 correspond to *p*-values less than the risk level, 0.05 implying that the mean SD differences between the two groups are statistically significant for the EIGEN-CG03C model.

Table 30. The *t*-test results for EIGEN-CG03C based on LAGEOS 2 data.

Variable	Diff (mean SD)	Diff. (SD)	*t*-value	*p*-value
Var 1 vs. Var 2	0.000762	0.012549	0.76336	0.446393
Var 1 vs. Var 3	-0.001170	0.013784	-1.06735	0.287453
Var 1 vs. Var 4	0.000778	0.012646	0.77322	0.440555
Var 2 vs. Var 3	-0.001933	0.008310	-2.92330	0.003976
Var 2 vs. Var 4	0.000016	0.001819	0.10920	0.913180
Var 3 vs. Var 4	0.001948	0.008341	2.93607	0.003824

The results for the *t*-test as derived from the four orbital tests using AIUG-CHAMP01S and LAGEOS 2 are presented in Table 31. These results however, indicate that the differences in the mean SD for each condition are not statistically significant (since $p \geq 0.05$).

Table 31. The *t*-test results for AIUB-CHAMP01S based on LAGEOS 2 data.

Variable	Diff (mean SD)	Diff. (SD)	*t*-value	*p*-value
Var 1 vs. Var 2	0.000143	0.009214	0.195760	0.845049
Var 1 vs. Var 3	0.000243	0.009204	0.333253	0.739385
Var 1 vs. Var 4	0.000169	0.009250	0.230246	0.818199
Var 2 vs. Var 3	0.000100	0.001663	0.759639	0.448603
Var 2 vs. Var 4	0.000026	0.001485	0.219537	0.826515
Var 3 vs. Var 4	-0.000074	0.001488	-0.630220	0.529461

Table 32 summarises the *t*-test results for the EGM2008 gravity field model based on LAGEOS 2 data. The results indicate that the differences in the mean SD between the first five groups are not statistically significant (i.e. $p \geq 0.05$). Similar results are obtained for the AIUB-GRACE01 gravity field model using LAGEOS 2 data, see Table 33. In both cases the difference in the mean SD between Var 3 versus Var 4 groups are statistically significant since $p \leq 0.05$.

Table 32. The *t*-test results for EGM2008 based on LAGEOS 2 data.

Variable	Diff (mean SD)	Diff. (SD)	*t*-value	*p*-value
Var 1 vs. Var 2	0.000278	0.009269	0.37783	0.706065
Var 1 vs. Var 3	0.000411	0.009389	0.55250	0.581384
Var 1 vs. Var 4	0.000141	0.009568	0.18556	0.853026
Var 2 vs. Var 3	0.000134	0.001317	1.27969	0.202532
Var 2 vs. Var 4	-0.000137	0.001615	-1.06938	0.286529
Var 3 vs. Var 4	-0.000271	0.001463	-2.33254	0.020934

Table 33. The *t*-test results for AIUB-GRACE01S based on LAGEOS 2 data.

Variable	Diff (mean SD)	Diff. (SD)	*t*-value	*p*-value
Var 1 vs. Var 2	0.000460	0.009136	0.63494	0.526388
Var 1 vs. Var 3	0.000326	0.009217	0.44596	0.656240
Var 1 vs. Var 4	0.000579	0.009249	0.78940	0.431059
Var 2 vs. Var 3	-0.000134	0.001715	-0.98588	0.325697
Var 2 vs. Var 4	0.000119	0.001650	0.90935	0.364550
Var 3 vs. Var 4	0.000253	0.001298	2.45936	0.014997

Figure 20 compares the gravity field models found to exhibit O-C mean SD differences that are statistically significant. In particular, for LAGEOS 1 data only the combined gravity field model GRIM5C1 has *t*-values corresponding to *p*-values less than the 0.05 risk level. The *p*-value for Var 2 versus Var 4 is however too close to the significant level hence the difference in the mean SD of the O-C is likely to have arisen by chance. In this case it becomes difficult to firmly conclude anything about the statistical significance of the mean difference (additional data processing is needed to ascertain the findings). The small *p*-values obtained for EIGEN-CG03C when analysing LAGEOS 2 data imply that the findings are unlikely to have arisen by chance. In fact the difference in the mean SD of the O-C between Var 2 versus Var 3 and Var 2 versus Var 4 tide parameterization tests are highly statistically significant since $p \leq 0.01$. Similarly, the *p*-values computed from the *t*-test using the O-C residuals derived from LAGEOS 2 data based on the EGM2008 and AIUB-GRACE01S models indicate that there are almost true differences in the mean SD between Var 3 versus Var 4 tide parameterization tests.

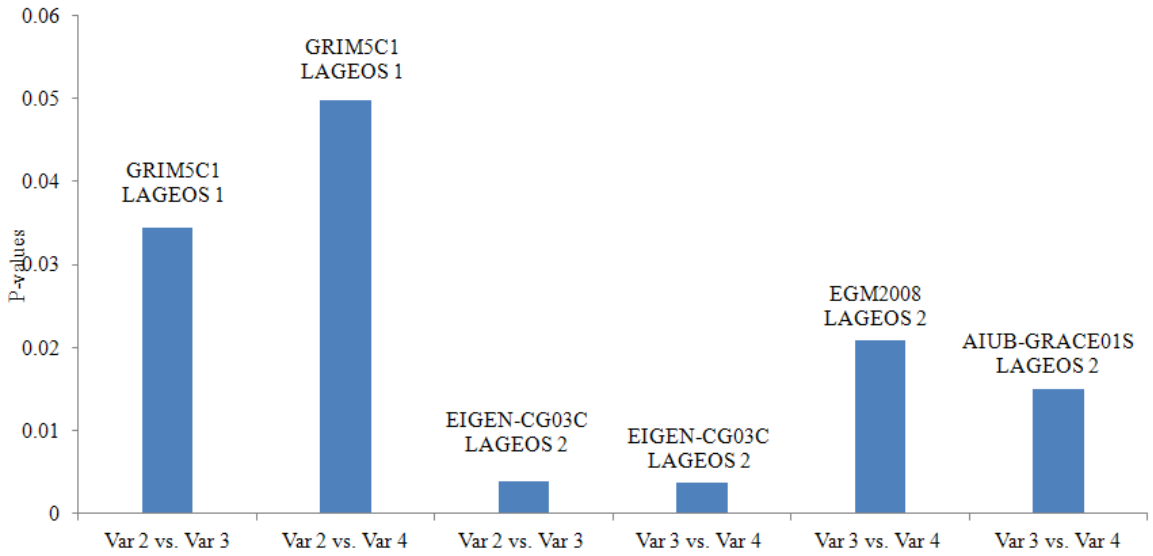

Figure 20. Comparisons of gravity field models showing mean statistical significant differences between Earth tide and pole tide models.

5.7. Concluding remarks

In this chapter the influence of tide parameterization on the accuracy of five gravity field modes is analysed. In particular, the tide parameterization effects on the accuracy of gravity field models in SLR data analysis is determined by studying the influence of solid Earth tides (modelled by IERS1, IERS2, IERS3 and IERS2010 pole tide standard model) on O-C residuals (with applications in POD) based on the selected gravity field models. In the SLR data analysis using the SDAS package the IERS1, IERS2, IERS3 and pole tide models have been used alternately (parameterized) in order to investigate how the O-C residuals are affected by the choice of the tide model set and across different gravity field models. The results indicate that the accuracy of the final orbital solution when using EIGEN-CG03C, AIUB-CHAP01S and EGM2008 and LAGEOS 1 data require the inclusion of spherical harmonic components due to Earth and pole tides to those of the gravity field models. Similar conclusions can be made for the GRIM5C1, AIUB-CHAMP01S and EGM2008 models when using LAGEOS 2 data. Since the computed mean SD across the four parameterizations based on the five gravity field models was statistically close a *t*-test was performed to assess whether the differences in the mean SD of the O-C were significantly different. The *t*-tests between most of the considered parameterization options are found to have *p*-values which were greater than the significant

level 0.05 (or 5%). Based on these results it can be concluded that the differences in the mean SD between the considered parameterization options for the selected gravity field models are not statistically significant. In particular, the differences in the mean SD of the O-C based on EIGEN-CG03C, EGM2008 and AIUB-GRACE01S and LAGEOS 2 data are unlikely to have arisen by chance as they exhibit statistically significant mean SD differences. In particular the small *p*-values obtained for EIGEN-CG03C imply that the differences in the mean SD are highly statistically significant. The deviation of EIGEN-CG03C from the expected is difficult to explain. This model produces expected results for IERS1, IERS2 and IERS3 (pole tide disabled), but produces an anomaly when processing for LAGEOS2 with IERS3 enabled and pole tide disabled. This distorts the graph of average values as contained in Figure 18. These distortions are possibly due to outliers in the O-C time series as presented in appendix A5, Figure 24 to Figure 33.

6. Geophysical applications of Earth's oblateness parameter J_2

Physics is mathematical not because we know so much about the physical world, but because we know so little; it is only its mathematical properties that we can discover, Bertrand Russell, 2009.

6.1. Introduction

The Earth's oblateness (J_2) is an important geophysical parameter derived from SLR data analysis. In the present chapter, J_2 computed by SDAS has been validated and found to be in close agreement with the J_2 value published in the literature. Additionally, the geophysical linkage of J_2 with the LOD and Atmospheric Angular Momentum (AAM) has been studied and confirmed by use of a data adaptive analysis methodology called the Empirical Mode Decomposition (EMD) reported by Wang *et al*., (2010). In particular, the oscillatory components known as the Intrinsic Mode Functions (IMFs) of J_2, LOD and AAM were derived and phase synchronization used to infer the geophysical linkage between J_2, LOD and AAM. The phase synchronization results demonstrate that there is some degree of synchronization between the signal components of J_2 and LOD and J_2 and AAM. A higher degree of phase synchronization is particularly observed for high frequency IMFs of J_2, LOD and AAM. Additionally, IMFs components that depict a weak or nil phase synchronization are believed to be mostly due to inherent noise components.

6.2. Background

The Earth is a complex dynamic system driven by various geophysical processes as reported by for example Dickey *et al*. (2002). These processes act to redistribute the mass of Earth and as a result influence the basic movement of the solid Earth relative to the geocentre, as well as causing spatial and time-dependent variations of the gravitational field of the Earth. An important spherical harmonic coefficient of the gravity field is the zonal harmonic of degree 2 and order 0, i.e. $-C_{20}$ which is equivalent to J_2. This coefficient is known to be related to the flattening of the Earth as well as to the angular spin velocity Ω (this is connected to the equatorial and polar moments of inertia given by (A) and (C) respectively) (Chao, 2006).

Considering the equatorial and polar moments of inertia, the J_2 coefficient can be expressed as in Equation (91) as reported in Chao (2006),

$$J_2 = \frac{(C - A)}{Ma^2}. \tag{91}$$

Equation (91) contains the difference of the polar greatest moment of inertia C and the equatorial minimum moment of inertia A normalized by Ma^2, where M and a are the Earth's mass and mean equatorial axis respectively. A further expression of J_2 relating to dynamic oblateness may be written as in Equation (92),

$$J_2 = \left[C / Ma^2\right]\left[(C - A)/C\right] \equiv \eta H, \tag{92}$$

In Equation (92), $\eta \equiv C / Ma^2$ is a fundamental function of the Earth's internal structure and $H \equiv (C - A)/C$ is the dynamic oblateness (the dynamic oblateness can be determined from the observation of the astronomical precession of the Earth). Knowing the estimated values of J_2 one can use the following relation to calculate the normalized values of C_{20} as shown in Equation (93),

$$\bar{J}_2 = -\bar{C}_{20} = -\sqrt{5}\overline{C_{20}}. \tag{93}$$

The estimated J_2 coefficient as determined from geodetic measurements may be given by Equation (94) (Cheng *et al.*, 1997)),

$$\begin{aligned} J_2 = -J_2^{(0)} &= \left[C - \frac{1}{2}(A + B)\right]\left(\frac{1}{Ma_0^{\,2}}\right). \\ &= (1082639.9 \pm 0.1) \times 10^{-9} \end{aligned} \tag{94}$$

The Earth oblateness parameter J_2 has attracted a lot of interest from the scientific community since the detection of its temporal variations over two decades ago. In particular, some studies have reported on significant temporal variability exhibited by this coefficient. For example, Yoder *et al.* (1983) reported a secular decrease of the trend in J_2 which was suspected to be associated with PGR effects. An increasing trend in J_2 which later reversed to its normal decreasing trend in the beginning of 1998 was reported by Cox and Chao (2002). The authors estimated the decrease in J_2 between 1979 and 2002 to be approximately -2.8×10^{-11} yr^{-1}.

The variability of J_2 has also been linked to variations observed in other geophysical parameters. One such parameter is the LOD which characterizes the variability of the Earth's rotation rate. Variations in LOD are due to contributions from surface mass loading changes as well as changes of the horizontal surface stress (torques). Surface mass loading variations are due to changes in atmospheric surface pressure, continental water storage (including snow and ice on land), and ocean bottom pressure (Chen *et al*., 2000). In contrast, the horizontal surface stress variations reflect the exchange of angular momentum between the solid Earth and the surrounding geophysical fluids e.g., wind and ocean current variations (Chen *et al*., 2000). The changes due to the combined atmospheric wind and surface pressure effects (i.e., the AAM) which arise from the mass re-distribution and the movement within the Earth system is known to be the dominant contributor (~90%) to the observed LOD variability (Chen 2005b).

Variations in the LOD are often modelled by two terms i.e., the mass and motion components as reported in Bourda (2008). The physical manifestation of the mass term (this is due to dynamic processes within the Earth) is modelled by the gravitational effects associated with the Earth's mass re-distribution. Most of the dynamic Earth processes that are associated with the temporal variations of the Earth's gravitational field are also linked to the variability of the Earth's rotation, through the temporal changes in LOD (Gross, 2003). Theoretically, the LOD variations are thought to be slightly proportional to changes in degree-2 spherical harmonic coefficients of the gravity field (Eubanks, 1993; Gross *et al*. 2004). The response to the LOD variability can approximately be given by Equation (95) as reported in Chen (2005b),

$$-\frac{\Delta LOD}{LOD_{mean}} = m_3(t) = \chi_3, \tag{95}$$

where ΔLOD are the changes in the LOD with respect to the mean LOD, LOD_{mean} is given by 86400 seconds, and χ_3 is the LOD excitation which includes the surface mass load change term $\left(\chi_3^{mass}\right)$ and the atmospheric winds or currents term $\left(\chi_3^{motion}\right)$.

In a case where a gridpoint (i.e., latitude φ, longitude λ and time t) is given the LOD excitations due to surface mass load fluctuations χ_3^{mass} and winds or currents motion χ_3^{motion} can be computed by using Equations, (96) and (97), all reported in Chen (2005b)

$$\chi_3^{mass} = \frac{0.753\bar{R}^4}{C_m g}\iint P\cos^3\varphi d\lambda d\varphi, \tag{96}$$

$$\chi_3^{motion} = \frac{0.998\bar{R}^3}{C_m g \Omega} \iiint U \cos^2 \varphi dp d\lambda d\varphi, \tag{97}$$

where $\bar{R} = 6.371 \times 10^6$ m and $\Omega = 7.292115 \times 10^{-5}$ rad-s^{-1} are the mean radius and mean angular velocity of the Earth, respectively. Furthermore $g \approx 9.81$ ms^{-2} is the mean gravitational acceleration, $C_m \approx 7.1236 \times 10^{37}$ kg m^2 is the third principal moment of inertia of the Earth's mantle, and P and U are the atmospheric surface pressure (mass term) and the zonal velocity (e.g., wind or ocean currents) respectively (Chen, 2005b). The surface mass change is often represented by the spherical harmonic coefficient of a geopotential depicted in Equation (98).

$$\begin{Bmatrix} \Delta C_{nm} \\ \Delta S_{nm} \end{Bmatrix} = \frac{R_e^{\,2}}{(2n+1)M} \iint \Delta\sigma(\theta,\lambda) \bar{P}_{nm}(\sin\theta) \cdot \begin{Bmatrix} \cos m\lambda \\ \sin m\lambda \end{Bmatrix} \cos\theta d\theta d\lambda. \tag{98}$$

In Equation (98), C_{nm} and S_{nm} are the degree n and order m normalized harmonic coefficients of mass decomposition, $\Delta\sigma(\theta,\lambda)$ is the surface mass load with $\Delta\sigma = \Delta P / g$ and M is the mass of Earth and $\bar{P}_{nm}$ is the 4π normalized associated Legendre function given by Equation (99),

$$\left[\frac{(2-\delta_{m0})(2n+1)(n-m)!}{(n+m)!} \right]^{1/2} \times P_{nm}. \tag{99}$$

The associated Legendre function of degree 2 and order 0 can be expressed as in Equation (100)

$$P_{2,0} = \frac{(3\sin^2\theta - 1)}{2}. \tag{100}$$

Applying the normalization factor given by Equation (99) to Equation (100) the normalized associated Legendre function of degree 2 and order 0 can be written as

$$\bar{P}_{2,0} = \sqrt{5} \cdot \frac{(3\sin^2\theta - 1)}{2}. \tag{101}$$

Based on Equation (95), the relationship between the LOD excitation with respect to the surface mass term χ_3^{mass} and the zonal harmonic spherical harmonics, $-C_{20}$ can be obtained by combining Equations (96) and (101) (Chen, 2005b and Bourda, 2008),

$$\chi_3^{mass} = \frac{0.753\bar{R}^2 M}{(1+k_2^{'})C_m} \cdot \frac{2}{3}\left(\Delta C_{00} - \sqrt{5}\Delta C_{20}\right). \tag{102}$$

Here M is the mass of the Earth, $k_2^{'} = -0.301$ is the degree-2 load Love number and C_{00} represents the total mass change of a given component normalized by mass of the Earth, i.e., $C_{00} = \Delta M / M$.

The motion part of the AAM component can be related to changes in LOD by Equation (103) (Bourda, 2008)

$$\frac{\Delta LOD_{winds}(t)}{LOD_{mean}} = \frac{h_{3\text{winds}}(t)}{C_m \Omega}, \qquad (103)$$

where h_3 is the axial relative angular momentum of the Earth corresponding to the winds or motion term. The linkage between J_2 and LOD is an important scientific investigation because of the geophysical applications in areas such as hydrology, atmosphere and ocean coupling. One way to establish the association between J_2 and LOD is to investigate the possible coherence of various modes of oscillation in the J_2 coefficient with those estimated from LOD fluctuations. Additionally, since the variations in LOD are also closely linked to those in the AAM it then follows that some modes of oscillation of J_2 could be synchronized with those of the AAM as reported in Sole *et al*. (2007). In the present analysis of phase synchronization, we investigate the linkage between J_2 and LOD as well as J_2 and AAM, based on the independent oscillatory components obtained from each of these geophysical parameters.

6.3. Inter-comparisons between SDAS estimated J_2 and a priori J_2 of EGM96, GRIM5C1, GGM03C and AIUB-GRACE01S models.

In the present study, the robustness of the analysis of SLR data by use of the SDAS package parameterization has been tested generally by comparing the values of unnormalised *a-priori* and estimated J_2 values based on the EGM96, GRIM5C1, GGM03C and AIUB-GRACE01S gravity field models. The purpose of the analysis was to validate J_2 computed from SLR data analysis using SDAS against the published values from the five selected gravity field models. Here the published J_2 values for each gravity field model and results obtained by using SDAS are summarized in Table 34 and Table 35. During processing the *a-priori* J_2 values are set as starting points in the estimation, and the formal errors of the GGM being used is set as the

estimation parameter constraint. The least-squares solution of J_2 is therefore constrained fairly tightly. Figure 21 depicts a comparison between *a-priori* J_2 values and those derived from SDAS data analysis based on the EGM96, GRIM5C1, GGM03C AND AIUB-GRACE01S gravity field models. In particular the plotted values are the differences between the normalized *a-priori* J_2 values and the SDAS derived J_2 based on LAGEOS 1 and 2 across the considered gravity field models. The results presented in Figure 21 indicate that the *a-priori* J_2 and the SDAS derived J_2 exhibits similar patterns and are in good agreement for all the GGMs as processed using LAGEOS 1 and 2 data.

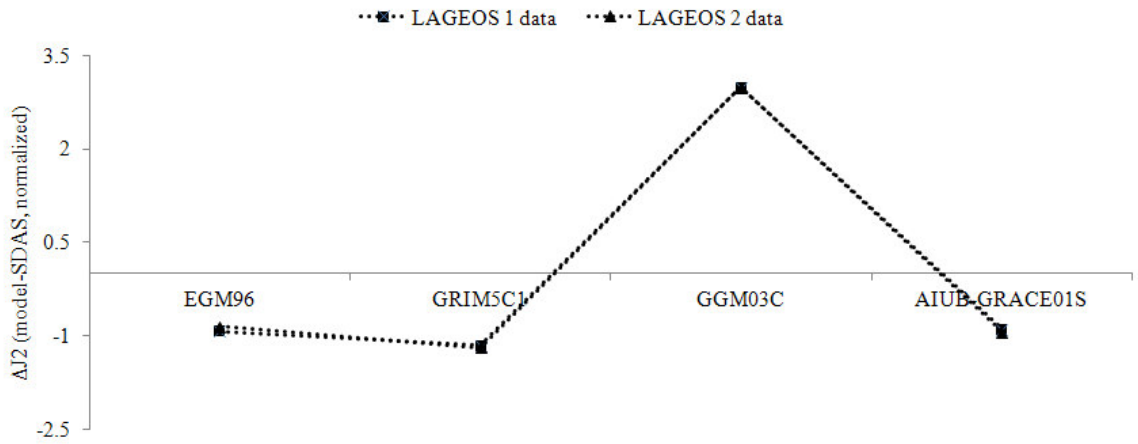

Figure 21. Comparison between *a-priori* J_2 values and those derived from SDAS data analysis. The plotted values are the differences between a priori J_2 values and SDAS derived in the normalized form.

As illustrated in Table 34 and Table 35, based on LAGEOS 1 and 2 data sets, the percentage differences (absolute) between the *a-priori* and SDAS estimated J_2 are in the order of 10^{-8} for all the considered GGMs. These results therefore suggest that the J_2 derived from SDAS could be used to compute normalized J_2 values that would be very similar to the published ones. No attempts were made to adjust *a-priori* values for $\dot{J}_2$ as the uncertainties in $\dot{J}_2$ are at the formal error level for the particular models used. Therefore one must consider that the epoch of the GGMs are not neccessarily those of the mid-epoch period of the processed SLR data (December

2005 to December 2008). Nevertheless, the SDAS package provides reasonable estimates with the J_2 *a-priori* values differing at the 10^{-10} to 10^{-11} level.

Table 34. Comparisons of *a- priori* J_2 from the five GGMs and J_2 derived from SDAS based on LAGEOS 1 data.

Model	A priori $J_2 \times 10^{-3}$	Formal error$\times 10^{-11}$	SDAS $J_2 \times 10^{-3}$	SDAS formal error $\times 10^{-11}$	$\Delta J_2 \times 10^{-10}$ (Model -SDAS)
EGM96	-1.0826267	3.561063	-1.0826268	7.8449	1.19859
GRIM5C1	-1.0826261	0.409800	-1.0826262	0.9162	1.69544
GGM03C	-1.0826355	4.684600	-1.0826368	0.1024	0.12672
AIUB-GRACE01S	-1.0826267	0.504104	-1.0826270	1.1270	2.66310

Table 35. Comparisons of *a-priori* J_2 from the five GGMs and J_2 derived from SDAS based on LAGEOS 2 data.

Model	A priori $J_2 \times 10^{-3}$	Formal error$\times 10^{-11}$	SDAS $J_2 \times 10^{-3}$	SDAS formal error $\times 10^{-11}$	$\Delta J_2 \times 10^{-10}$ (Model - SDAS)
EGM96	-1.0826267	3.561063	-1.08262673	7.8902	6.54752
GRIM5C1	-1.0826261	0.409800	-1.0826263	0.7634	1.19854
GGM03C	-1.0826355	4.684600	-1.0826369	0.1023	0.13675
AIUB-GRACE01S	-1.0826267	0.504104	-1.0826268	1.1268	1.19356

6.4. Geophysical modes of oscillation inherent in LOD, AAM and J_2

In this section the linkage between J_2 and LOD as well as J_2 and AAM geophysical parameters is investigated by use of a recent, widely used data adaptive analysis methodology, the EMD described in Huang *et al.* (1998). The data used to extract oscillation components of J_2 are the same as that presented in Chapter 4 for the EGM96, GRIM5C1, GGM03C and AIUB-GRACE01S models. The LOD data used in this study is the official IERS EOP 08 C04 product series archived and freely available from ftp://hpiers.obspm.fr/iers/eop. The LOD data are computed from VLBI, GPS and SLR space geodetic techniques. Similarly, the AAM data used in the present study were the National Centers for Environmental Prediction (NCEP) effective atmospheric angular momentum functions calculated from NCEP/NCAR (National Center for Atmospheric Research) reanalyses archived on pressure levels. The AAM data are

freely available at the geophysical fluid: the Special Bureau for the Atmosphere (SBA), ftp://ftp.aer.com/pub/anon_collaborations/sba. For the purpose of this work both the LOD and AAM data period were matched with the analysed period of SLR observations. Properties of the J_2, LOD and AAM were analysed using a modified Ensemble Empirical Mode Decomposition (EEMD) method reported in e.g., Botai *et al.* (2009) and Zhaohua and Huang (2009).

The EEMD methodology is a data adaptive method of decomposing a series into local oscillatory components called the IMFs originally reported in Zhaohua and Huang (2009). According to Zhaohua and Huang (2009), an IMF is a mono-component signal that satisfies two conditions:

1. In the whole data set, the number of extrema and the number of zero crossings must either equal or differ at most by one;
2. At any point, the mean value of the envelope defined by the local maxima and the envelope defined by the local minima is zero.

The EEMD method is a variant of the original EMD developed by Huang *et al.* (1998). This method is used for analysing non-stationary and non-linear signals driven by underlying linear and non-linear stochastic processes. In general, the EMD method extracts oscillatory components from a given series by an iterative procedure known as the *sifting process* (SP). Here for any given data, a signal is decomposed into a series of IMFs generated at each scale starting from smooth to coarse and a residual representing a trend function. According to Huang *et al.* (1998), the EMD algorithm can be summarized as follows:

1. For a given data denoted by $x(t)$, identify all the local extrema.
2. Interpolate all the maxima and minima with natural cubic splines lines to form the upper $u(t)$ and lower, $l(t)$, envelopes.
3. Compute the mean of the envelopes: $m(t) = \dfrac{\left[u(t) + l(t)\right]}{2}$.
4. Take the difference between the data and the mean as the proto-IMF: $h(t) = x(t) - m(t)$.
5. Check the proto-IMF against the definition of the IMF and the stoppage criterion to determine if it is an IMF.

6. If the proto- IMF doe not satisfy the IMF definition then repeat steps 1 to 5 on $h(t)$ until it satisfies the definition.
7. If the proto- IMF satisfies the definition, assign the proto- IMF as an IMF component, $c(t)$.
8. Iterate on the residue, $f(t) = x(t) - c(t)$, as on the data. This process will end when the residue reaches a non-existence of extrema.

The flow chart of the sifting process is depicted in Figure 22.

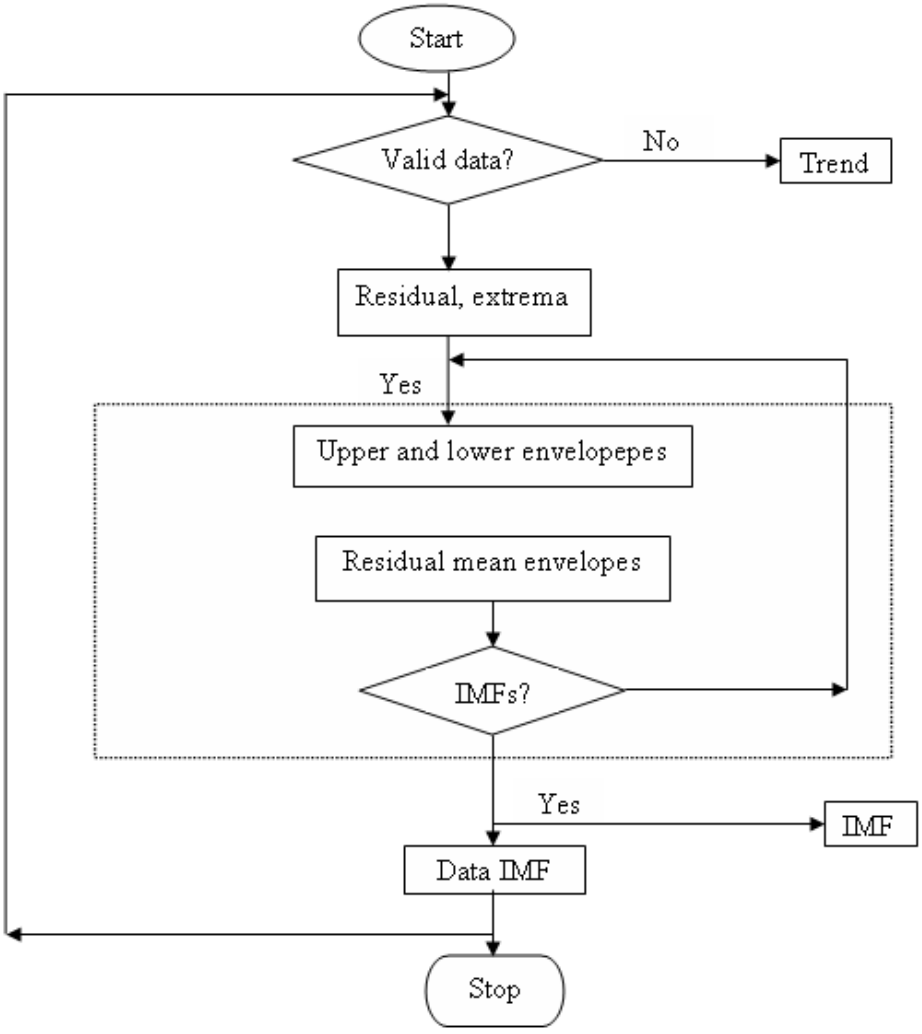

Figure 22. The flow chart of the decomposition process of EMD through the sifting procedure (adapted from Wang *et al*., 2010).

Mathematically, the sifting process can be described as follows in Equation (104)

$$\begin{aligned} &x(t)-m_{1,1}(t)=h_{1,1}(t);\\ &h_{1,1}(t)-m_{1,1}(t)=h_{1,2}(t);\\ &\quad\cdots\\ &\quad\cdots\\ &h_{1,k-1}(t)-m_{1,k}(t)=h_{1,k}(t).\\ &\Rightarrow\ h_{1,k}(t)=c_1(t) \end{aligned} \tag{104}$$

Here the indices indicate the iteration of the same step. It then follows that

$$\begin{aligned} &x(t)-m_{1,1}(t)=h_{1,1}(t);\\ &h_{1,2}(t)=h_{1,1}(t)-m_{1,2}(t)=s(t)-(m_{1,1}+m_{1,2});\\ &\cdots\\ &\cdots\\ &h_{1,k}(t)=h_{1,k-1}(t)-m_{1,k}(t)=x(t)-(m_{1,1}+m_{1,2}+\ldots+m_{1,k});\\ &\Rightarrow\ c_1(t)=x(t)-(m_{1,1}+m_{1,2}+\ldots+m_{1,k}). \end{aligned} \tag{105}$$

The step presented here serves to extract the first IMF component. Subsequently, one finds that

$$\begin{aligned} &x(t)-c_1(t)=r_1(t);\\ &r_1(t)-c_2(t)=r_2(t);\\ &\cdots\\ &\cdots\\ &r_{r-1}(t)-c_n(t)=r_n(t). \end{aligned} \tag{106}$$

Thus for any given data, the signal $x(t)$, can be decomposed by the EMD method as

$$x(t)=\sum_{j=1}^{n}c_j(t)+r_n(t), \tag{107}$$

where c_j represents the j^{th} IMF and r_n is the residual.

In the present analysis of the oscillatory mode decomposition of J_2, LOD and AAM the following algorithm steps (is illustrated in Figure 23) were followed:

a) Compute IMFs by use of a noise assisted data analysis method based on Zhaohua and Huang (2009).
b) Determine significant IMFs based on the energy criterion.
c) Compute the phase difference of the analytic signals of the selected IMFs.

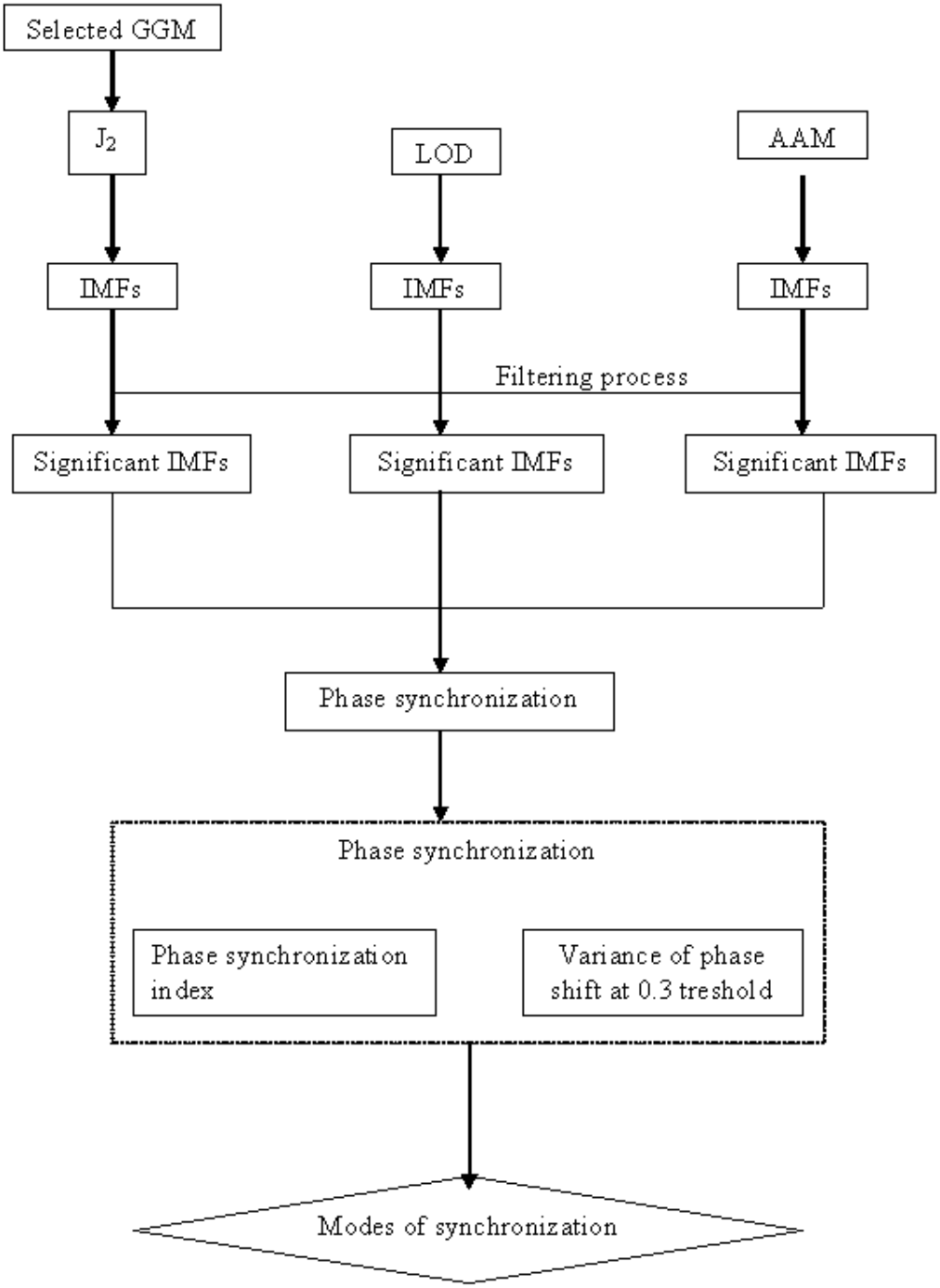

Figure 23. Synchonization method used in the current study.

In this work, only significant IMFs were selected to investigate the association of J_2 oscillatory components with those from LOD and AAM. The significant IMFs were selected based on the energy criteria: their energy ought to be within the inter-quartile range of the IMF with maximum energy from a total of 10 IMFs decomposed adaptively by use of 0.33σ noise level with 50 ensembles. Intrinsic Mode Functions with small instantaneous amplitudes/energy and high frequencies were considered as outliers.

6.4.1. Analysis of phase synchrony

In order to quantify the level of synchrony across the recorded IMFs from J_2, LOD, and AAM geophysical parameters the Phase Locking Value (PLV) approach reported in Sole at al. (2007) was used. In particular, for two signals $x(t)$ and $y(t)$ of equal time length with instantaneous phase $\Phi_x(t)$ and $\Phi_y(t)$ respectively, the PLV bivariate metric is given by Equation (108),

$$PLV = e^{i\Delta\Phi_{xy}(t)} = \left| \frac{1}{N} \sum_{j=1}^{N} e^{\left(i\left(\Phi_x(j\Delta t) - \Phi_y(j\Delta t)\right)\right)} \right|, \qquad (108)$$

where Δt is the sampling period and N is the number of points in the sampling period of each signal.

The corresponding IMFs extracted from J_2 (based on four selected gravity field models), LOD and AAM were analyzed to detect the level of interaction between J_2 and LOD as well as J_2 and AAM mode signals. Here we only consider phase locking as an important factor and impose no restrictions on the amplitudes. In general, a phase locking ratio of 1:2 was considered appropriate for our analysis. Furthermore, we calculate the variance of the phase shift and determine the degree of phase synchronization based on a 0.3 threshold. The usage of this low threshold cut-off is to eliminate IMFs that primarily consist of noise. Generally, the frequencies ω_x and ω_y of any two given periodic oscillators are related by $n\omega_x = m\omega_y$ where n and m are integers. If a phase for each oscillator is defined by Equation (109),

$$\phi_j(t) = w_j t, \qquad (109)$$

then the principle of phase synchronization corresponds to a phase locking between two oscillators defined by Equation (110),

$$\varphi_{n,m} = \left| n\phi_X(t) - m\phi_Y(t) \right| \leq C, \qquad (110)$$

where ϕ_X and ϕ_Y are the unwrapped phases of the signals of the two oscillators and this is equivalent to a constant, C. Equation (110) can now be used to derive the phase synchronization index defined in Equation (111) as reported in Hutt *et al*. (2003) and Allefeld and Kurths (2003),

$$\gamma_m(t) = \frac{1}{\tau}\sqrt{\left(\sum_{i=-\tau/2}^{\tau/2}\cos\left(\Delta\phi_m(t+i\Delta T)\right)\right)^2 + \left(\sum_{i=-\tau/2}^{\tau/2}\sin\left(\Delta\phi_m(t+i\Delta T)\right)\right)^2}. \qquad (111)$$

Here τ denotes the number of time points in the sliding window of width ΔT. The computed variance normally varies between 0 and 1, i.e., $0 \leq \gamma_m \leq 1$. Assuming that $\phi_m(t)$ represents the difference between two phases that change at certain times, then $\gamma_m(t)$ can be used to define the phase synchronization index. It follows that the maximum value of $\gamma_m(t) = 1$ would indicate a perfect synchronization between phases with phase difference ϕ_m. Similarly, a zero phase synchronization between phases with phase difference ϕ_m would be achieved when $\gamma_m(t) = 0$.

The phase synchronization results between signal components extracted from J_2 and those extracted from LOD and AAM can be found in Appendix A6, Figure 34 to Figure 49. Visual inspection of these figures suggests that there exists some degree of synchronization between J_2 signal components and those from LOD and AAM. In particular, ~70% of the signal components extracted from J_2 data show a high degree of synchronization with those derived from LOD and AAM signals. The higher phase synchronization seems to be located at the high frequencies in the case of J_2 and LOD and J_2 and AAM. The presence of synchronization between J_2 components and components from LOD and AAM suggests that the LOD and AAM signal components are embedded in the data hence confirming that the two parameters are related as stated in the literature. Pairs showing high synchronization between J_2 from LAGEOS 1 and 2 data and LOD and AAM are summarized in Table 36 and Table 37 respectively. The calculated phase synchronization index for these pairs ranges between 0.01 and 0.3 based on phase locking ratio of 1:2. Components showing weak behaviour of asynchrony or no synchronization at all between J_2 and LOD and AAM respectively could be a

result of random noise between the signal components of the interacting signals or irregular variability in the J_2 signal.

Table 36. Phase synchronization pairs showing a high degree of synchronization between J_2 and LOD.

J_2 derived from LAGEOS 1 based on model	Synchronized pairs between J_2 and LOD
EGM96	δ_{14}, δ_{15}, δ_{17}, δ_{35} and δ_{47}
GRIM5C	δ_{13}, δ_{14}, δ_{17}, δ_{34} and δ_{47}
GGM03C	δ_{13}, δ_{14}, δ_{17}, δ_{34} and δ_{47}
AIUB-GRACE01S	δ_{14}, δ_{15}, δ_{17}, δ_{35} and δ_{47}
J_2 derived from LAGEOS 2 based on model	Synchronized pairs between J_2 and LOD
EGM96	δ_{14}, δ_{17}, δ_{24} and δ_{67}
GRIM5C	δ_{14}, δ_{17}, δ_{24}, δ_{47} and δ_{77}
GGM03C	δ_{14}, δ_{17}, δ_{24}, δ_{47} and δ_{77}
AIUB-GRACE01S	δ_{14}, δ_{17}, δ_{24}, δ_{27} and δ_{67}

Table 37. Phase synchronization pairs showing a high degree of synchronization between J_2 and AAM.

J_2 derived from LAGEOS 1 based on model	Synchronized pairs between J_2 and AAM
EGM96	δ_{11}, δ_{13}, δ_{16} and δ_{26}
GRIM5C	δ_{11}, δ_{13} and δ_{16}
GGM03C	δ_{11}, δ_{13}, δ_{16} and δ_{26}
AIUB-GRACE01S	δ_{11}, δ_{13}, δ_{16} and δ_{26}
J_2 derived from LAGEOS 2 based on model	Synchronized pairs between J_2 and AAM
EGM96	δ_{11}, δ_{13}, δ_{16} and δ_{26}
GRIM5C	δ_{11}, δ_{13} and δ_{16}
GGM03C	δ_{11}, δ_{13} and δ_{16}
AIUB-GRACE01S	δ_{11}, δ_{13}, δ_{16}, δ_{26} and δ_{65}

6.5. Concluding remarks

The oscillatory components in the SDAS derived J_2 coefficient based on EGM96, GRIM5C1, GGM03C and AIUB-GRACE01S gravity field models were investigated using SLR data from LAGEOS 1 and 2 for a period of about 3 years (i.e. December 2005 to December 2008). A data adaptive analysis method, EMD was utilized to decompose the J_2, LOD and AAM signals into significant IMFs. The phase synchronization between J_2 and LOD and J_2 and AAM signal components show that there exists some degree of synchronization between the interacting

signals. A higher degree of phase synchronization is observed at high frequencies of J_2, LOD and AAM decomposed IMFs. Components showing a weak or nil phase synchronization are believed to be primarily contaminated by random noise within the signals.

7. Conclusion and recommendations for future research

"Nothing is too wonderful to be true, if it be consistent with the laws of nature" Michael Faraday.

7.1. Summary

Earth gravity field models (these are empirical models that are used to explain the nature of the gravity field of Earth) have significant applications in geodesy, geophysics, oceanography and navigation. In particular, precise gravity field models have been used in:

- The determination of accurate orbits of both low and high orbiting satellites, this is a pre-requisite for the launch, navigation, prediction and tracking of artificial orbiting satellites,
- Precise estimation of the global unified geoids particularly the oceanic geoids,
- Understanding geophysical phenomena of the Earth's interior as well as geodynamic processes associated with the lithosphere and mantle composition,
- Establishment of a global height reference system for datum connection and
- Understanding mass transportation and different distributions within the Earth system through detection and assessment of spatial-temporal variations of the gravitational field of the Earth.

Nowadays several gravity field models derived exclusively from SLR tracking measurements or/and from a combination of SLR measurements with surface gravity measurements (e.g. terrestrial gravity data and airborne gravity data) and satellite radar altimetry measurements have been freely released to the scientific community for research. These models however exhibit certain inaccuracies due to various factors ranging from the type of utilized satellite data, availability and quality of the data, global coverage, accuracies of force models incorporated in the geodetic data analysis, etc. Recent satellite missions such as CHAMP, GRACE and GOCE are believed to have the capability to resolve the long- and medium wavelength features of the Earth's gravity by providing new data for precise and high resolution gravity field modelling. Since the inception of the three satellite missions a number of gravity field models have been derived and some of the old ones have been modified. These progresses in gravity field modelling require that the models be constantly assessed and validated. Despite the many

scientific milestones in gravity field modelling, studies focusing on evaluating the accuracy of the gravity field models in the context of POD using SLR data have remained in-exhaustive. The research work reported in this thesis evaluates various gravity field models in terms of the O-C range residuals, investigates the influence of SLR analysis parameterization on the accuracy of the gravity field models and demonstrates the capability of the SDAS package to investigate the different gravity field models for POD. It is of importance to emphasize that the results presented in this thesis are related to spherical harmonic coefficients up to degree and order 20 as proxies for gravity field models.

7.2. Concluding remarks

The main aim of this research was to evaluate the accuracy of gravity field models used for POD by use of LAGEOS 1 and 2 data collected from ILRS tracking stations. The research began by providing an historical overview of gravity field models intended to highlight the development of gravity field models and their scientific applications. An investigation in general improvement in the gravity field modelling based on the O-C residuals derived from LAGEOS 1 and 2 data using various selected gravity field models was presented in Chapter 4. In Chapter 5 of the thesis we performed a sensitivity analysis on the O-C residuals computed from LAGEOS 1 and 2 tracking data considering 5 gravity field models. The main focus was to investigate the effects of different tide parameterizations on the O-C residuals across different gravity field models. In Chapter 6, some of the SDAS derived products are validated and analysed for geophysical applications. In particular, the J_2 spherical harmonic coefficient derived from the SDAS package was compared with the coefficients published in the literature. In addition, association of the J_2 coefficient with other geophysical parameters (LOD and AAM) was also investigated. Based on the analysis of results presented in this research work the following conclusions can be drawn:

- The development of gravity field modelling over the period of evaluation (15 years) has generally improved. In particular, based on the seven months analysis of SLR data, the accuracy of the evaluated gravity field models depict an improvement by a factor of at least 2 since 1990 in terms of O-C range residuals. The analysis of the O-C residuals reveals that the accuracy of gravity field models released from 1999 onward are

approximately at the same level of accuracy (within the limits of sensitivy of our tests as described in this work), although there are many specific differences amongst most recent gravity field models. A further analysis (for a period of three years) of a set of four gravity field models released between 1996 and 2008 demonstrate slight differences in their O-C range residuals. Overall, in the SLR data analysis (this includes the seven months and ~3 years of LAGEOS 1 and 2 SLR data) undertaken in this study, it was found that the satellite-only derived gravity field model AIUB-GRACE01S could be the most accurate due to the low SD of the corresponding O-C range residuals.

- The influence of tide parameterization (using IERS1, IERS2, IERS3 and IERS2010 pole tide standard model) on the accuracy of five gravity field models was analysed based on LAGEOS 1 and 2 data. The results indicate that the accuracy of the final orbital solution when using EIGEN-CG03C, AIUB-CHAP01S and EGM2008 and LAGEOS 1 data require the inclusion of spherical harmonic components due to Earth and pole tides to those of the gravity field models. Similar results were found for the GRIM5C1, AIUB-CHAMP01S and EGM2008 models when using LAGEOS 2 data. Statistical *t*-tests were performed to assess whether the differences in the mean SD of the O-C are significantly different. Most of the considered parameterization options are found to have *p*-values which are greater than the significant level 0.05 (or 5%) implying that the differences in the mean SD for the selected gravity field models are not statistically significant. Differences in the mean SD of the O-C based on EIGEN-CG03C, EGM2008 and AIUB-GRACE01S and LAGEOS 2 data are unlikely to have arisen by chance. In particular the small *p* values obtained for EIGEN-CG03C imply that the differences in the mean SD are highly statistically significant. In the case were the *p*-values are found to be relatively low but still greater than 0.05 (e.g. $p = 0.08$ for AIUB-GRACE01 and GRIM5C1 based on LAGEOS 1 and 2 data respectively) more data need to be processed to draw firm conclusions.
- The J_2 coefficients derived from the SDAS package are comparable to those published in the literature. Furthermore, the presence of a geophysical signal component in the time-variable J_2 coefficient was assessed by use of the phase synchronization between J_2 and LOD and J_2 and AAM. Our analysis revealed that there exists some degree of

synchronization between the J_2, LOD and AAM signal components. A higher degree of phase synchronization is observed in the high frequency modes of J_2, LOD and AAM of the IMFs obtained from the empirical decomposition of considered time series (J_2, LOD and AAM). Components showing a weak or nil phase synchronization are believed to be primarily contaminated by random noise within the signals.

7.3. Recommendations

7.3.1. Assessment of additional SLR LAGEOS data

A vast quantity of LAGEOS 1 and 2 tracking data ought to be processed to robustly infer the general improvement of gravity field modelling. Gravity field models derived from as early as the 1970's to the most recent (2011/2012) need to be considered in order to track fully the progress in gravity field modelling. Additional investigation involving larger SLR data sets can be valuable in assessing significant accuracy and resolution of the various considered gravity field models.

7.3.2. Probing the significance of SLR parameterization

In this thesis the tidal deformation effects due to IERS Earth and pole tides (models) on the O-C residuals across 5 different models were investigated. The three models (IERS1, IERS2, IERS3 and IERS3 with pole tides disabled) considered are used to correct for the effects of Earth and pole tides on the spherical harmonice coefficients of the GGMs in question. These effects are directly linked to the O-C residuals which represent the orbits of the satellites. However, there are many other factors that affect the orbit solution and hence gravity field models. These include the atmospheric delay/loading, ocean loading, tropospheric effects, displacements caused by solid Earth tides, general relativistic effects, etc. In order to achieve an improved orbit solution these parameters/effects require full understanding in terms of their contributions to precise satellite orbit determination. It is therefore recommended that sensitivity analysis be extended to include these parameters/effects.

7.3.3. Additional satellites

Nowadays the satellite based global gravity field determination is based on three techniques (e.g. continued GNSS tracking, K-band range and range-rate tracking and satellite gradiometry) which involve CHAMP, GRACE and GOCE satellite missions. High accuracy gravity field determination through these satellite missions is attributed to their orbit attitude, observational mode and on-board equipments. The new satellite missions overcome the SLR drawbacks such as uneven orbit tracking by ground stations non-uniform SLR observations. Consequently, evaluation of global gravity field model accuracies can be expanded by processing long term data sets from these satellite missions. Results from these new satellite missions can then be compared to those obtained in this thesis using LAGEOS 1 and 2 data. Other possible satellites to be considered may include those at a greater range of altitudes and inclinations, e.g. Stella and Starlette.

7.3.4. Technical issues

Much needs to be done to improve the quality and distribution of the available data. For example, the state of the ILRS network needs to improve. The network requires more sites, a better geometry, better tracking capabilities, and enhanced data acquisition capabilities. Thus gaps in the Southern Hemisphere and Africa in particular need to be filled with some SLR tracking stations for a more complete data set for validation purposes.